METEOROLOGICAL APPLICATIONS
Meteorol. Appl. **21**: 94–104 (2014)
Published online 29 November 2012 in Wiley Online Library
(wileyonlinelibrary.com) DOI: 10.1002/met.1350

Modelling of wind shear downwind of mountain ridges at Hong Kong International Airport

David Carruthers,[a]* Andrew Ellis,[a] Julian Hunt[a] and P. W. Chan[b]
[a] *Cambridge Environmental Research Consultants (CERC), UK*
[b] *Hong Kong Observatory, Kowloon, Hong Kong*

ABSTRACT: A theoretical and computational study is presented of the wind flow over the mountain ridges to the south of Hong Kong International Airport given the upwind profiles of 'mean' velocity and temperature. A sensitivity study shows how large variations in wind speed, wind shear and wind direction occur on the approach path when the upwind flow from the southeast is stably stratified above the boundary layer with a significant inversion no more than a few hundred metres above the ridge (height about 450 m). The Froude number is close to unity. The effects of vertical wind shear across the inversion layer reduce the speed-up, and directional wind shear changes the surface flow direction. The observed horizontal length scales along the approach are about equal to the projected widths of the predominant features of the ridges and valleys. For an extreme wind event there was found to be satisfactory agreement between the wind speed measured by a landing aircraft and the predictions of the fast quasi-linear analytically based computer model FLOWSTAR. This suggests that near real time application of the model and near real time monitoring with remote and *in situ* instruments can be used to predict these extreme flow events and hence give warnings about them. Conclusions are drawn about how such predictive modelling could be developed.

KEY WORDS airflow; complex terrain; wind shear; elevated inversion

Received 16 January 2012; Revised 27 April 2012; Accepted 10 July 2012

1. Introduction

Significant wind shear at Hong Kong International Airport (HKIA), situated on Lantau Island, mostly occurs as a result of disruption of the prevailing airflow by the mountains typically rising to about 450 m within 4 km of the southerly runway. A severe event (Chan, 2011) occurred on the morning of 27 December 2009, when seasonal easterly winds affected the south coast of China: this event was sufficiently serious that a number of aircraft were required to divert. An earlier report by Shun and Lam (2002) discussed the characteristics of the flow during a wind shear event at HKIA.

The variable wind speed and high wind shear near the runways are regularly monitored with radar, surface and airborne instruments and radiosondes. Numerical models have previously been used to help explain these complex flows (Cheung *et al*., 2008), but these models cannot be run in real time so as to provide operational forecasts over periods of a few minutes when the wind shear can become hazardous.

This paper reports on the application of an analytically based fluid flow computational modelling system, in this case FLOWSTAR (Carruthers *et al*., 1988), to the simulation of the complex airflow at HKIA in near real time using observed data. Unlike weather forecast and CFD models, the resolution used is not limited by the physics of the model and may be as small as required subject to the constraints of computational speed. Another model that has been used for predicting high winds at airports is that of Sheridan *et al*. (2004).

FLOWSTAR computes perturbations to the approach wind field using a steady state model. However, the solution can be iterated to adjust to local data on timescales as small as the time it takes for air to flow over the terrain and can account for large perturbations. The model has been considerably developed from the idealized studies of Jackson and Hunt (1975), Hunt and Snyder (1980) and Hunt *et al*. (1988), and has been applied to the calculation of power output of wind turbines in complex flows and dispersion of pollutants (TOPFARM, 2011). An advantage of this modelling approach is that many different conditions can be studied to help provide an overall understanding of types of flow and critical hazards, as shown in this paper.

This paper first summarizes, in Section 2, the features of flow over hills and mountains relevant to high speed flow phenomena at HKIA, Section 3 presents a discussion of FLOWSTAR and Section 4 presents the measured data and also data used as input to the model. In Sections 5 and 6 calculations using FLOWSTAR of airflow both over Lantau Island and in the vicinity of HKIA for the morning of 27 December 2009 are presented including sensitivity studies and comparisons with the in flight data, followed by a discussion in Section 7.

2. Characteristics of winds over complex ridges

2.1. Stratified flow over ridges

In the discussion of the different types of flow over ridges it is convenient to consider in turn different levels of stable stratification (Carruthers and Hunt, 1990).

* Correspondence to: D. Carruthers, Cambridge Environmental Research Consultants (CERC), Cambridge CB2 1SJ, UK.
E-mail: david.carruthers@cerc.co.uk

2.1.1. Neutral or weak stratification

Consider a smooth ridge of height H and half length L (which may be an undulation on a larger ridge) when the approach wind is perpendicular to the ridge and its velocity U (typically 5–10 m s^{-1}) is approximately uniform with height, except near the surface. At the inversion height the velocity $U = U_0$. It is assumed that the potential temperature is stable with buoyancy frequency N (typically $N < 0.015$ s^{-1}). Theoretical and experimental studies show that if the stratification is very weak, $\left(F_{\mathrm{L}} = \frac{U_0}{NL} > 1\right)$, then typically for smaller hills or undulations on a hill side ($L < 1$ km), the maximum positive perturbation to the wind speed (ΔU) is at the top of the hill and is proportional to the slope:

$$\Delta U \sim \frac{U_0 H}{L}, \tag{1}$$

(Jackson and Hunt, 1975; Hunt *et al*., 1988). If the maximum slope on the lee side is greater than about one third, the flow separates leading to a negative perturbation in wind speed that persists downwind. Typically, from a wake model and wind tunnel experiments (Counihan *et al*., 1974) the dependence with distance (x) for $x > 3H$ is:

$$\frac{\Delta U}{U_0} \sim \frac{3}{(x/H)}. \tag{2}$$

2.1.2. Moderate stratification

In this case the stratification is larger but is still weak enough at about the height of the mountain top that the flow has enough kinetic energy to pass over it, so that (Smith, 1979):

$$F_{\mathrm{H}} = \frac{U_0}{NH} > 1. \tag{3}$$

Then for large ridges, where $L >> H$ and when

$$\frac{1}{2} \lesssim F_{\mathrm{L}} \lesssim 1, \tag{4}$$

the maximum wind speed occurs on the lee slope and is typically

$$\Delta U \sim U_0 HN. \tag{5}$$

Further downwind, when $\frac{x}{L} > 2$, ΔU decreases because lee waves form above the hill. With greater stability or larger length, $F_{\mathrm{L}} < \frac{1}{2}$ the region of speed-up continues over the flat terrain (or the ocean at HKIA) far downwind of the mountain. This case has also been discussed by Lilly and Klemp (1979).

2.1.3. Strong stratification

If the stratification is strong enough that $F_{\mathrm{H}} < 1$ (which occurs typically when $H > 1$ km), as the flow approaches below the mountain top it does not have sufficient kinetic energy to rise over the top at lower levels. It slows down below a level approximately equal to $H(1 - F_{\mathrm{H}})$, and tends to move in horizontal planes around the mountain (see field and lab experiments reviewed by Snyder (1985)). For the flow that passes over the mountain, the speed-up is also controlled by wave motion (Hunt *et al*., 2006) and $\Delta U \sim U_0$ for all values of $F_{\mathrm{H}} < 1$. Downwind of the mountain the flow separates and $\Delta U \sim -U_0$.

2.1.4. Elevated inversion

In many atmospheric situations there is a stable inversion layer at $z = h_0$ in the flow approaching the mountain, i.e. there is a large potential temperature difference ΔT_i across a layer with thickness l_i much less than the mountain height.

The dynamical effect of the elevated inversion layer may be represented by an inversion height Froude number:

$$F_i = \frac{U}{\sqrt{g' h_0}} \tag{6}$$

where the reduced frequency $g' = g\frac{\Delta T_i}{T}$ and typically $g' \sim 0.1$ m s^{-2}. In the situations of most concern for high winds near ridges the inversion is above the ridge (i.e. $h_0 > H$), and the wind speeds are low enough and inversion high enough that $F_i < 1$. In this case as the flow accelerates over the mountain top the streamlines converge and therefore the inversion may descend. Then there are two possibilities: for very low wind speeds, if $F_i < F_i^* < 1$, where F_i^* is a critical value depending on H/h_0 the inversion is so strong that downwind of the summit, the streamlines rise and the flow decreases. For steep mountains the flow separates.

For greater wind speeds, $F_i^* < F_i < 1$, the wind speed at the hill top is great enough that the local Froude number:

$$F_i(x) = \frac{U_0 + \Delta U}{\sqrt{g' h(x)}} \sim 1, \tag{7}$$

then the flow descends and accelerates down the lee side of the ridge. There is no separation, and the flow takes the form of a strong low level jet: in some cases the flow streamlines may subsequently rise rapidly in the form of a hydraulic jump (Carruthers and Choularton (1982), denoted as CC). In general, an elevated inversion layer is accompanied by a deep stable layer above it with buoyancy frequency N. This effectively strengthens the inversion layer so that the combined inversion Froude number may be expressed as F_i^c, where:

$$F_i^c \simeq \frac{U_0}{\left[N^2 L^2 + g\left(\Delta T_i/T\right) h_0\right]^{\frac{1}{2}}} \tag{8}$$

2.1.5. Shear across the inversion layer

It is frequently observed that elevated inversion layers have large shears of both wind speed and wind direction across them (Lapworth, 2010). The theory of vortex sheets (e.g. Coelho and Hunt, 1989), shows such layers are strained by the accelerating and decelerating flow, $U(x)$, which thus affects how the velocity shear in an inversion layer varies over the mountain. In a steady state the changes in the velocity jump $\Delta u_i(x)$ are inversely proportional to the changes in the mean flow ΔU below the jump and:

$$\Delta u_i \approx -\Delta U_{0i} \frac{\Delta U}{U_0} \tag{9}$$

where ΔU_{0i} is the upstream change in velocity across the layer. Thus, the errors associated with neglecting upwind shear will be reduced where the flow speeds up (e.g. in strong downslope flows), but will be amplified where the flow slows down, (e.g. in wakes in neutral flow, and in the blocked flows on the upwind side of the mountain).

3. Features of FLOWSTAR

As discussed in the introduction FLOWSTAR is an analytically based model. It calculates the perturbation to the mean airflow and turbulence by taking account of changes in surface elevation and surface roughness. It takes account of the effects of stable stratification by representing the atmosphere as two distinct layers each with a different buoyancy frequency. These two layers represent the boundary layer and the free troposphere and may be separated by a temperature step to represent an elevated inversion, following CC (Figure 1). Of the flow categories considered in Section 2.1, FLOWSTAR is able to take account of each type of stratification (Sections 2.1.1, 2.1.2, 2.1.3) including the impacts of an elevated temperature inversion (Section 2.1.4), which is of most relevance to the current study.

The modelling system is essentially linear: however, some non-linearity is imposed through a non-linear surface condition for terrain elevation. Nevertheless FLOWSTAR is currently not able to take account of some significant non-linear effects, including hydraulic jumps, nor is it able to model the amplitude of trapped lee waves, which are damped to avoid singularities, nor wind shear across an elevated inversion. In neutral conditions there are limitations associated with separating flows which occur in the leeside for $h/L \sim 1/3$, however separation is suppressed where stable stratification is strong enough to significantly affect the flow over a hill but not strong enough to cause flow around a hill. This is the case for wind shear events at HKIA, and FLOWSTAR can be used for higher leeside slopes in such situations.

The computational speed of FLOWSTAR is very fast (much faster than CFD), depending mainly on the calculation of Fourier transforms and the analytical expressions for the flow perturbations. The spatial resolution of the model in the horizontal plane depends on the resolution of the terrain data that is available, whilst the solution is continuous in the vertical so that model output can be calculated at any specified height.

4. Data provided and FLOWSTAR model input

The following data were made available by Hong Kong Observatory for use in the modelling study:

1. topographical data for Hong Kong at 100 m resolution;
2. upper air ascent data at King's Park, Hong Kong for 0000 and 1200 UTC on 27 December 2009;
3. data from the surface based automatic weather stations in Hong Kong, and,
4. data from aircraft and LIDAR of airflow from the missed approaches of flights on 26 December.

4.1. Topographical data

Figure 2 shows a surface contour map of the Hong Kong territory obtained from the terrain elevation data provided. The location of the two runways at HKIA is shown. Figure 3 shows an isometric projection for Lantau Island. The figures clearly show the generally hilly terrain of the territory and the close proximity of the mountainous terrain immediately to the south east of HKIA.

4.2. Meteorological data

Figure 4 shows data from the radiosonde ascents from King's Park for 0000 UTC on 27 December 2009 (corresponding to 0800 on 27 December 2009 LST). The data shown are those that are directly measured, comprising the wind speed (U), wind direction and temperature, and also derived data comprising potential temperature and buoyancy frequency (N). The idealized profiles used in the base case model runs are also shown for wind speed and direction, and buoyancy frequency.

The wind direction is close to easterly near the surface but there is strong directional shear with the direction turning clockwise to near westerly at a height of 1700 m. The lowest layers in the boundary layer were close to neutrally stable (low potential temperature gradient and buoyancy frequency), however a very strong temperature inversion was present between about 600 and 900 m above mean sea level (amsl).

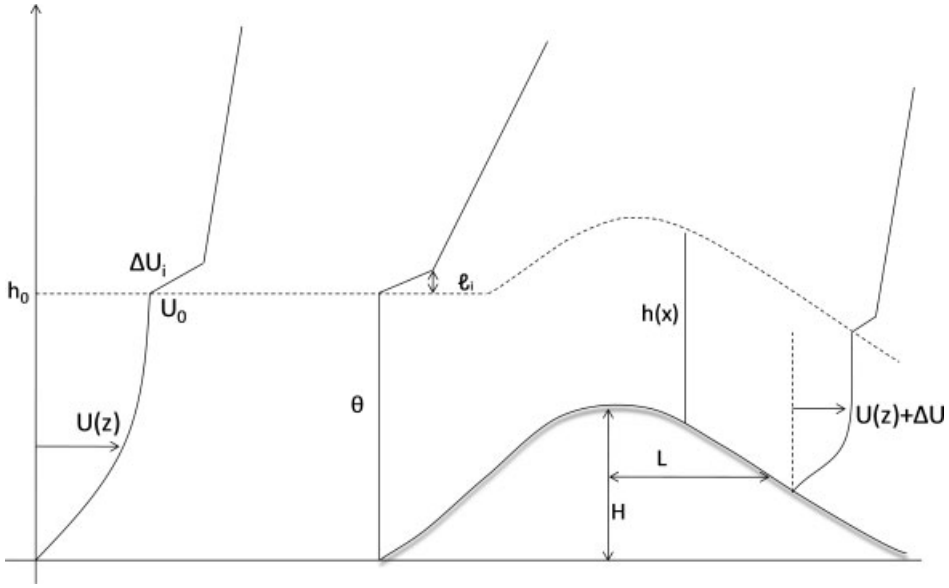

Figure 1. Schematic of flow over hill with elevated temperature inversion thickness l_i, height $h(x)$. The upstream vertical wind speed and potential temperature profiles are U and θ; ΔU is the perturbation in U over the hill.

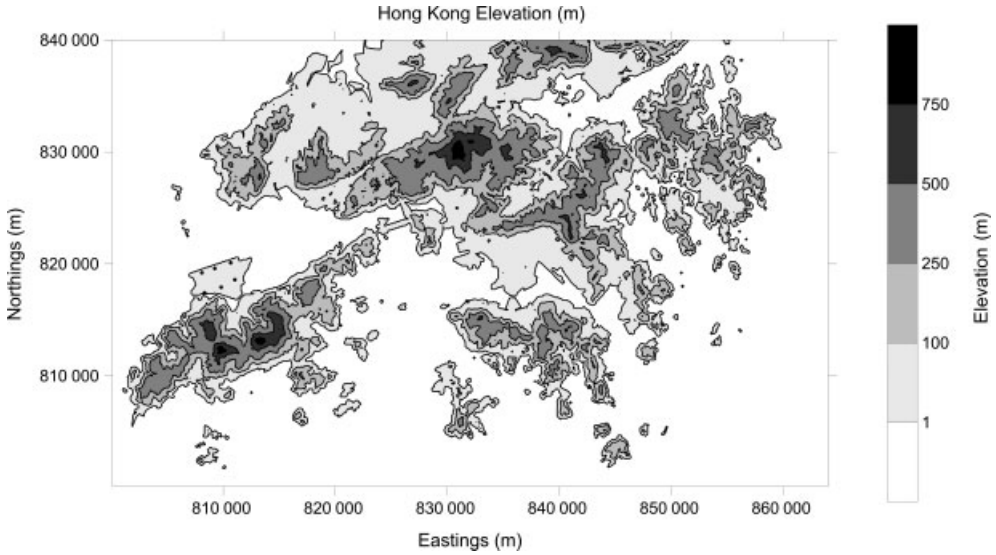

Figure 2. Surface Contour Map of Hong Kong. The black dots show the runway locations.

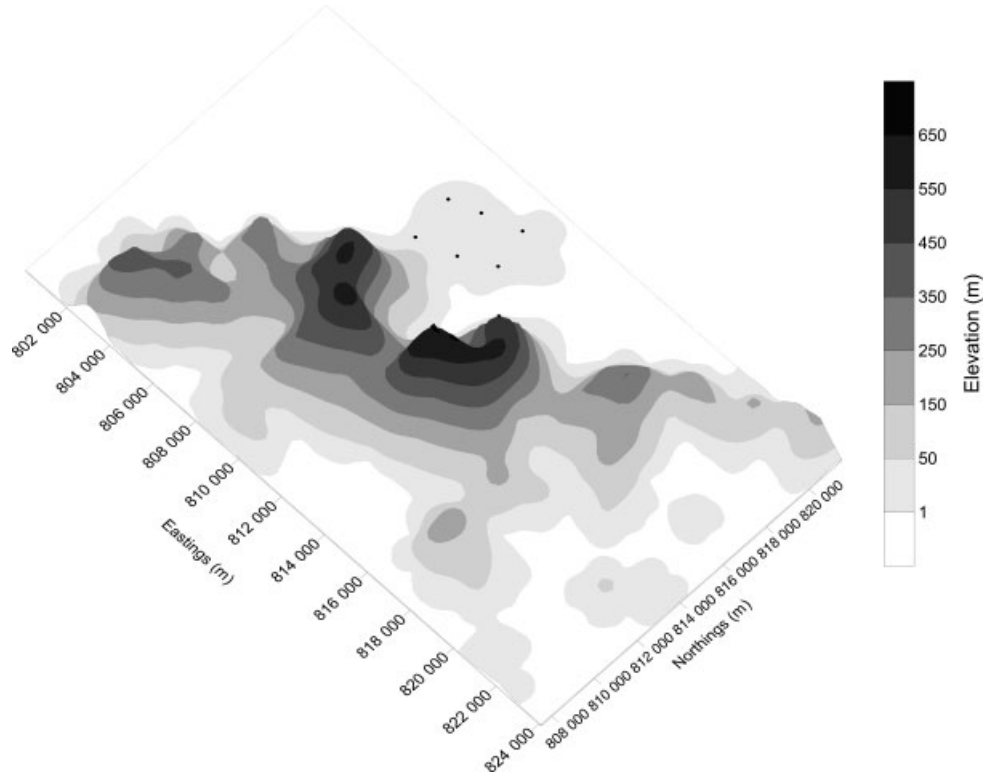

Figure 3. Isometric projection of Lantau Island. The black dots show the runway locations.

Figure 5 shows a limited selection of ascent data for 1200 UTC on 27 December 2009, specifically wind speed, wind direction and temperature. These data show that the wind speed had decreased by the time of this ascent and that the directional shear near the surface had increased so that there was no dominant wind direction.

4.3. Input data

Input to FLOWSTAR comprises terrain elevation, either on a regular or irregular grid and data used to determine the upstream vertical profiles of wind speed, turbulence and potential temperature. Minimum data requirements for this are wind speed and temperature at a specified height, cloud cover, Julian day, time of day and buoyancy frequency above any elevated inversion topping the boundary layer. However, derived parameters including boundary layer height and Monin-Obukhov length or surface heat flux may also be input directly into the model.

In this study the ascent data from King's Park for midnight on 27 December 2009 UTC were used to provide an estimate of the boundary layer height and buoyancy frequency above, whilst wind speed was determined by using the observed 10 m

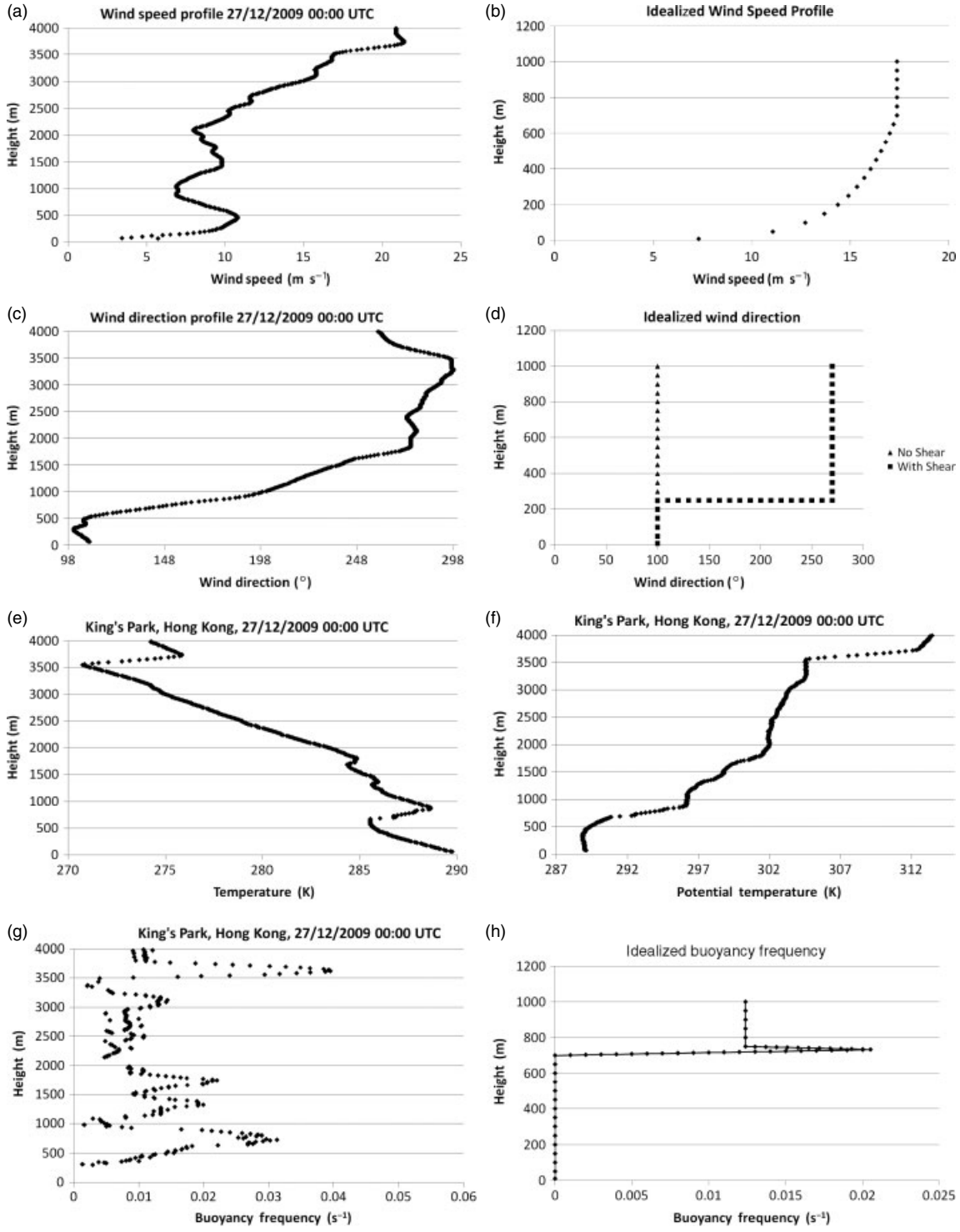

Figure 4. Observed, derived and idealized meteorological profiles at 0000 UTC, 27 December 2009 from a radiosonde released at King's Park, Hong Kong (a) Observed wind speed profile; (b) idealized wind speed profile; (c) observed wind direction profile; (d) idealized wind direction profile; (e) observed temperature profile; (f) derived potential temperature profile; (g) derived buoyancy frequency profile; and (h) idealized buoyancy frequency profile.

wind at Cheung Chau weather station on an island some 16 km southeast of HKIA, together with an estimate of the surface roughness at that site (0.5 m). Both the surface observation and ascent data were used to estimate wind direction. Wind speed data from the ascent data were not used due to the presence of high buildings and elevated terrain near King's Park which would impact on the wind speed (and wind direction) relatively near the ground. Three cases were considered. The first used the observed 10 m wind and direction and boundary layer height determined from the ascent data, the second, the wind direction within the inversion layer, and the third the wind direction within the inversion layer with the height of the boundary layer estimated as its height above the complex terrain (not upstream).

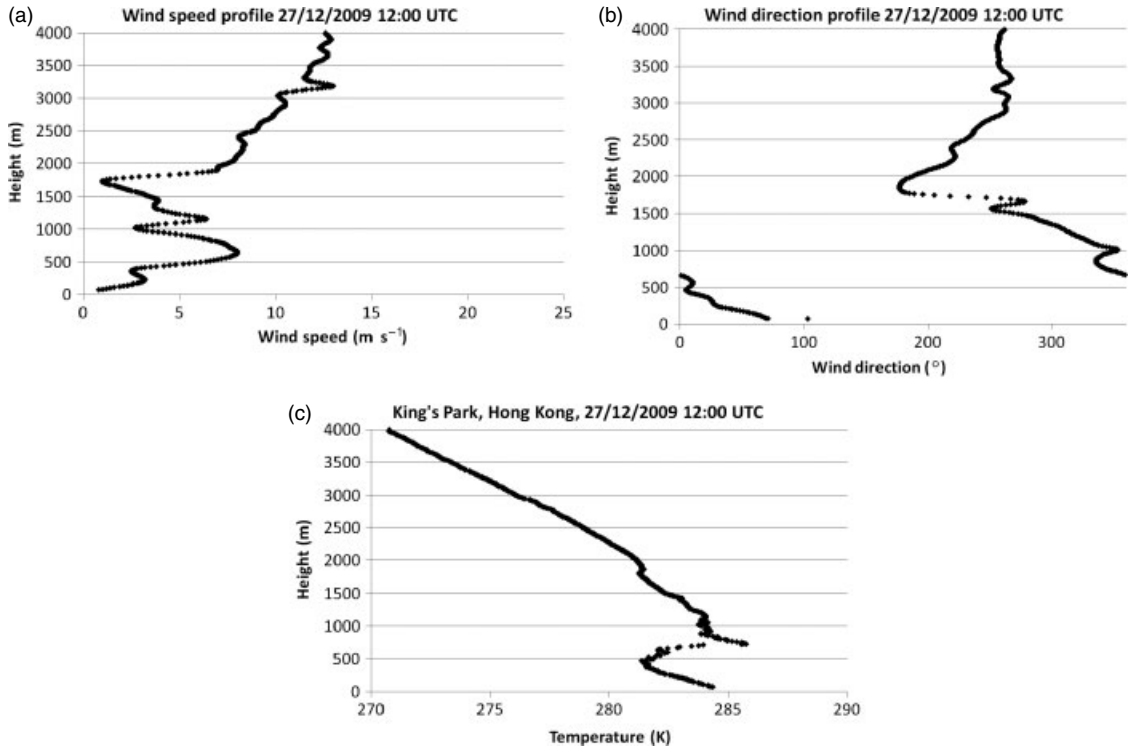

Figure 5. Observed meteorological data at 1200 UTC, 27 December 2009 from a radiosonde released at King's Park, Hong Kong (a) Wind speed profile; (b) wind direction profile; (c) temperature profile.

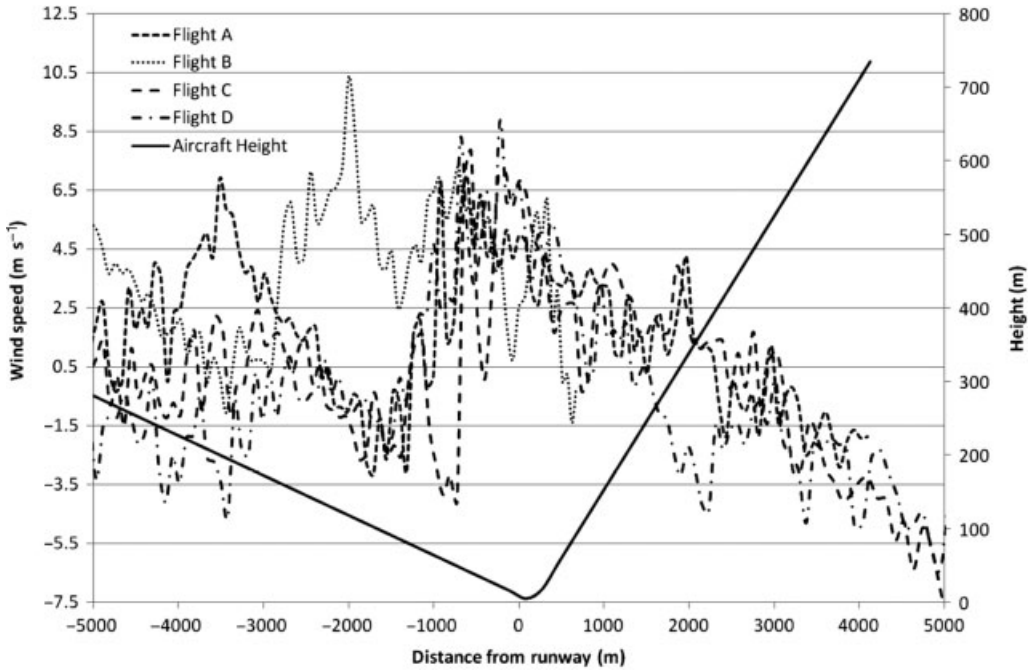

Figure 6. Measured head wind speeds from the missed approach of various flights on 26 December 2009.

The input conditions for the three cases are shown in Table 1.

4.4. Airflow data

Airflow data were provided from the missed approaches of a number of flights (A–D) on 26 December 2009 UTC. At this time, strong shear of both wind speed and direction were experienced by aircraft landing from the south west towards

Table 1. Model input parameter values for the three cases.

m s^{-1}	U (10 m)	Wind direction	L_o (m)	N (s^{-1})		ΔT (°C)	Z_o (m)
				$z < h_o$	$z > h_o$		
Case A	7.3	100°	865	0	0.0124	7.19	0.5
Case B	7.3	140°	865	0	0.0124	7.19	0.5
Case C	7.3	140°	400	0	0.0124	7.19	0.5

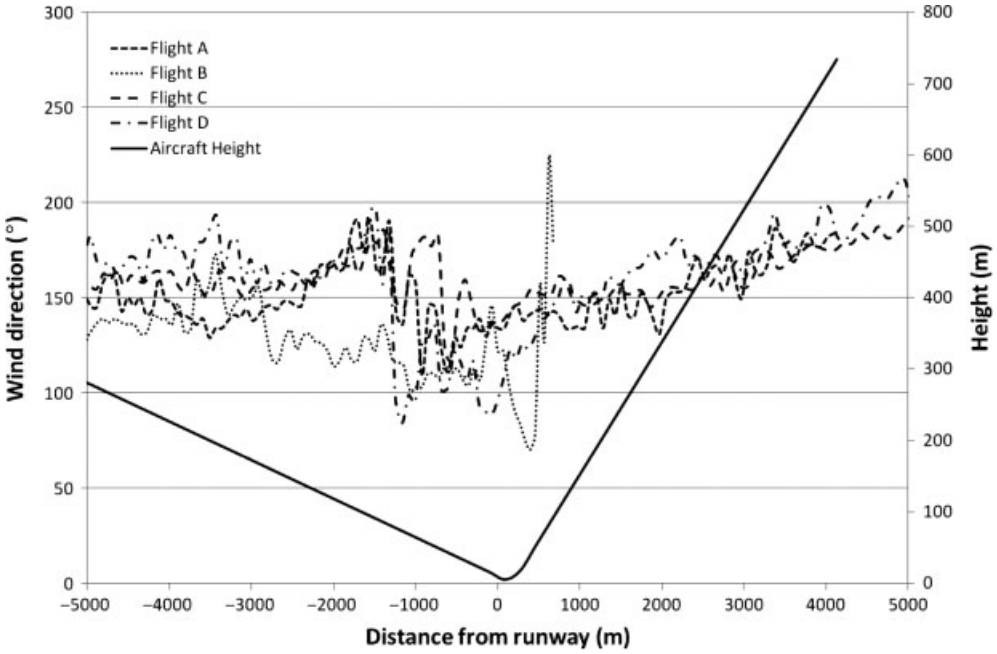

Figure 7. Measured wind direction from the missed approaches of various flights on 26 December 2009.

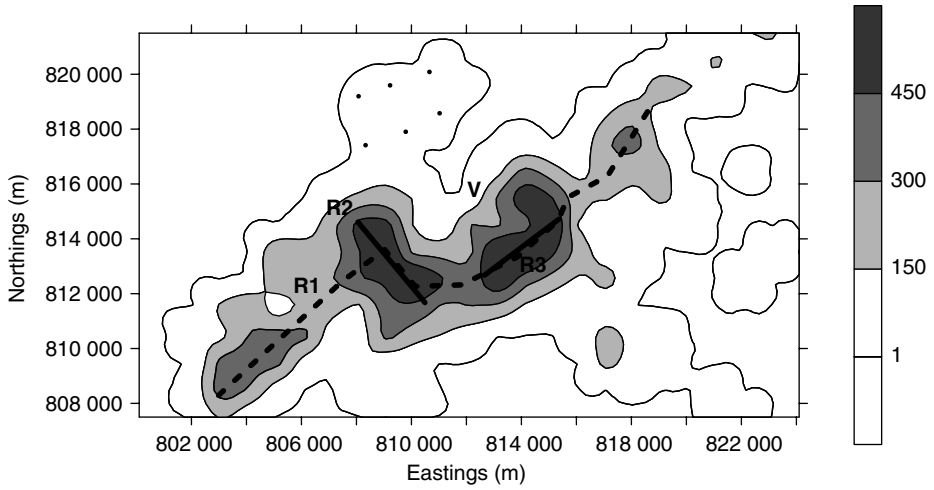

Figure 8. Surface Contour Map of Lantau Island. The black dots show the runway locations. The labels R1, R2 and R3 denote the three ridges described in the text and V denotes the valley, also mentioned in the text.

the southerly runway of the airport. See, for example, Figures 6 and 7 which show measured wind speed and wind direction, respectively, from various flights on 26 December 2009. The datum (distance = 0) is at the west end of the southerly runway.

5. Model runs

Figure 8 shows contours of a simplified form of terrain that has orographic features similar to those of the actual terrain of Lantau Island near the HKIA. In simple terms these consist of a ridge R_1 height H_1 in the southwest-northeast direction with additional sub ridges R_2 and R_3 with heights H_2 and H_3 rising above H_1. R_2 lies approximately perpendicular to R_1 with its NW end close to the west end of the southerly runway.

Table 2 shows calculated values for the composite, inversion layer and upper layer Froude numbers (see Section 2) derived from the input data for a range of inversion layer heights.

Table 2. Comparison of Froude numbers for various values of inversion height h_0..

Inversion height (m)	Composite Froude number, F_i^C	Inversion Froude number, F_i	Upper-layer Froude number, F_L
400	0.50	1.65	0.53
450	0.51	1.58	0.53
500	0.51	1.53	0.54
600	0.52	1.43	0.56
700	0.52	1.35	0.57
865	0.53	1.25	0.59

The length scale L is calculated as $2\pi/\overline{k}$ where $\overline{k}$ is the dominant wavenumber of the complex terrain in the downwind direction (in this case $L = 2500$ m), U_0 is the value of the

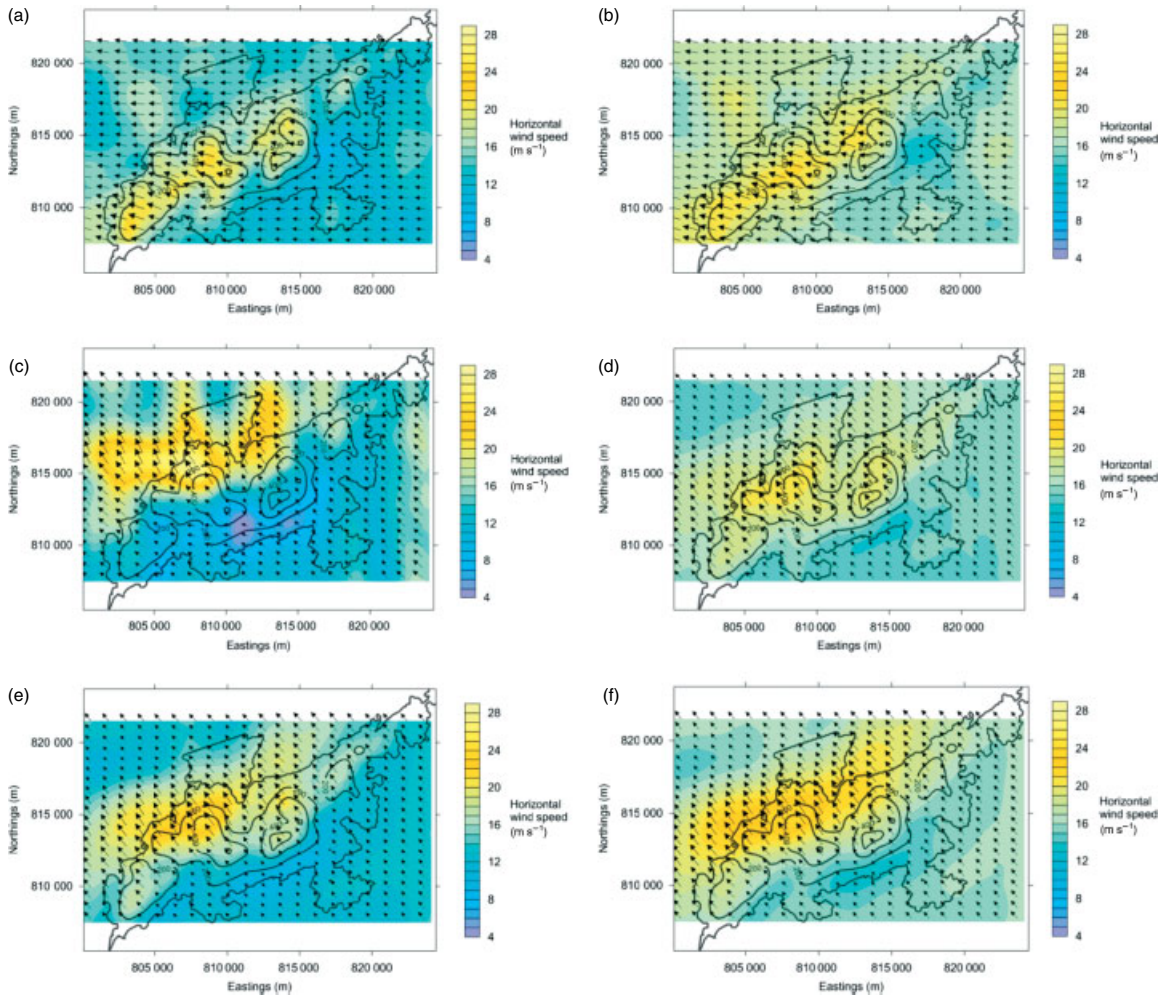

Figure 9. (a) Calculated airflow at 200 m above ground level for $\phi = 100^\circ$ and $h_0 = 865$ m. (b) Calculated airflow at 600 m above ground level for $\phi = 100^\circ$ and $h_0 = 865$ m. (c) Calculated air flow over Lantau Island at 200 m above ground for $\phi = 140^\circ$ and $h_0 = 865$ m. (d) Calculated air flow Lantau Island at 600 m above ground for $\phi = 140^\circ$ and $h_0 = 865$ m. (e) Calculated air flow over Lantau Island at 200 m above ground for $\phi = 140^\circ$ and $h_0 = 400$ m. (f) Calculated air flow over Lantau Island at 600 m above ground for $\phi = 140^\circ$ and $h_0 = 400$ m. The coloured contours show the magnitude of the horizontal wind speed. Note that (a) and (b) correspond to CASE A in Table 1; (c) and (d) correspond to CASE B in Table 1; (e) and (f) correspond to CASE C in Table 1.

wind speed in the upwind profile at height h_0. It can be seen that the combined Froude number $F_i^c \sim 0.5$ (Section 2.1.4) is consistent with strong downslope flow in the leeside of the ridges.

Figure 9 shows contour and vector plots of the horizontal component of the wind at 200 m above the ground (Figure 9(a), (c) and (e)) and at 600 m above the ground (Figure 9(b), (d) and (f)). The model runs show a complex flow pattern over Lantau Island and close to the southerly runway. In all the cases there is some upstream blocking and then acceleration down the leeside of the ridge before subsequent deceleration. This is most marked for Figure 9(b) when the wind direction is from 140°. Also of note are the streaks of high velocity which persist well to the north west of HKIA in Case B and which result in wind shear along the flight paths; similar features have been observed by LIDAR (Shun and Lam, 2002). These variations in the transverse direction are likely to be connected with the three dimensional nature of the ridge (i.e. the ridges R2 and R3 superimposed on the main ridge R1) and the superposition of internal gravity waves. Since the greatest speed-ups occur immediately downwind of the highest ridges and as ridge R_2 is very close to the runways, the highest wind speeds downstream of R_2 coincide with the runways. However, the flow downwind of ridge R_3 is fastest in the valley V and has already decelerated by the time it reaches the runways.

6. Model sensitivity to meteorological input data

A series of model runs was conducted to examine the sensitivity of the flow to boundary layer height and the wind direction of the approach flow. The parameter values were set within a reasonable range about the observed radiosonde measurements as these only give an indication of the vertical profile for a particular landing and take-off, since they are for a fixed moment in time and in addition are affected by topography in the vicinity of King's Park. The results are presented as the perturbation to the wind speed along the flight path of the aircraft approach to the southerly runway and also as total wind speed along the flight path, for direct comparisons with the measured speeds from aircraft on the landing approach.

6.1. Wind direction

Figure 10 shows the perturbation to the mean wind speed along the flight path for a range of wind directions ($\phi = 100^\circ$ to $\phi = 140^\circ$) for a fixed inversion height ($h_0 = 500$ m) and temperature jump ($\Delta T = 7.19\,^\circ$C). The calculations show that both the magnitude of the greatest perturbation in the wind speed and its location are highly dependent on the upstream wind direction, for example minima in headwind occur at 3000 m upstream and 1000 m downstream of the runway end for a wind direction of 130°, whilst they occur at about 7000 m and 500 m upstream for a wind direction of 100°. The range in the perturbation is typically more than 10 m s^{-1} between the peaks and troughs.

6.2. Inversion height

Given that the peak observed perturbation was close to the runway end ($x = 0$) when $\phi = 140^\circ$, these calculations suggest that a wind direction of about 140° is most representative of the approach flow. This is close to the direction observed at the height of the inversion layer. Therefore this wind direction was used to examine the sensitivity of the wind speed to inversion height (Figure 11) in which h_0 is varied from $h_0 = 400$ m to

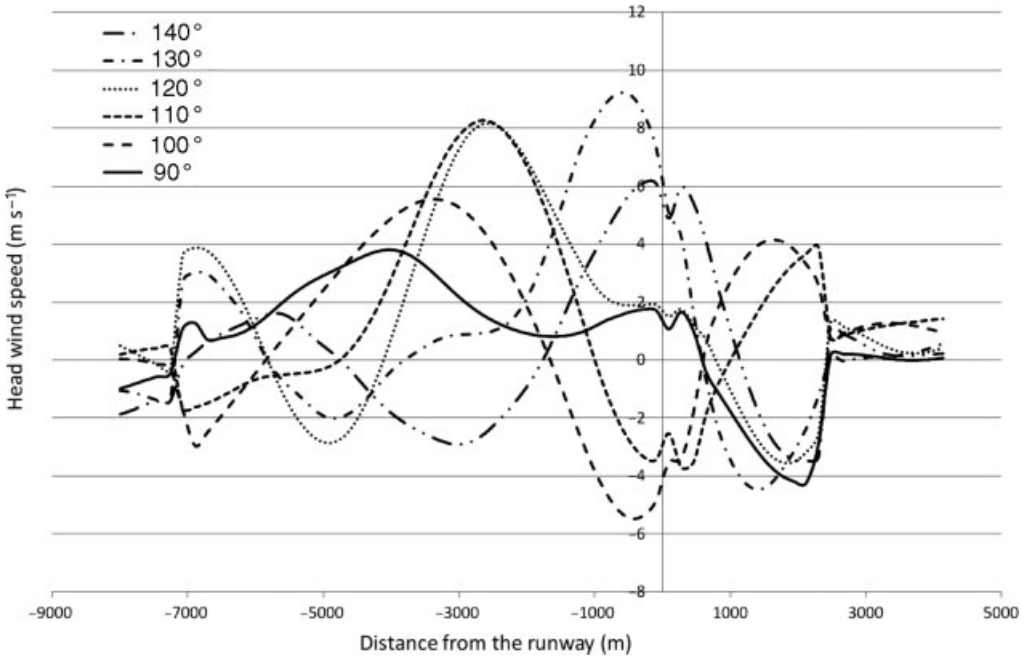

Figure 10. Perturbation to the head wind against distance from the runway (west end) for various wind directions. $h_0 = 400$ m and $\Delta T = 7.19\,^\circ$C.

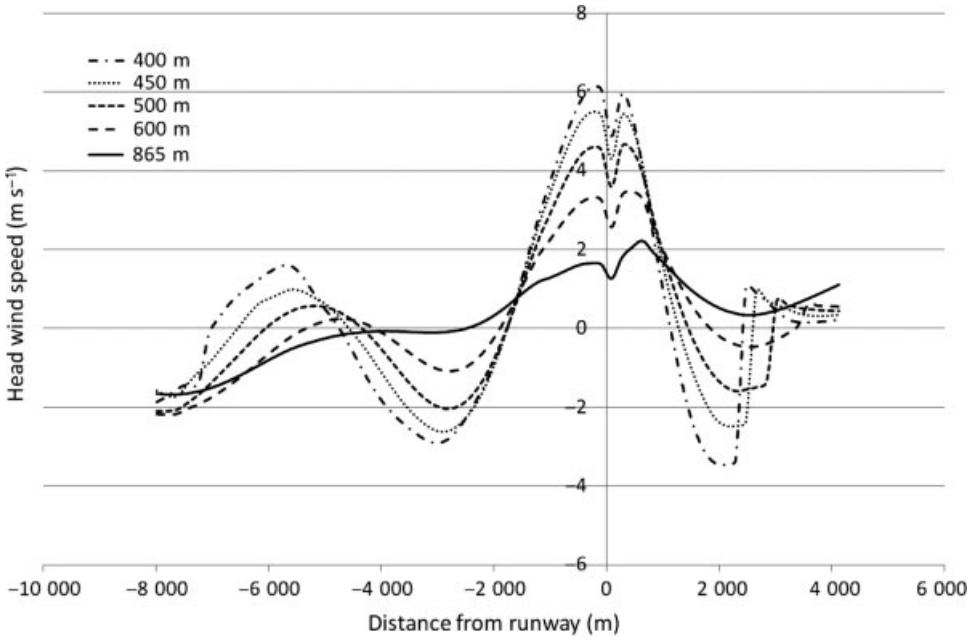

Figure 11. Perturbation to the head wind against distance from the runway (west end) for various inversion heights. $\phi = 140^\circ$ and $\Delta T = 7.19\,^\circ$C.

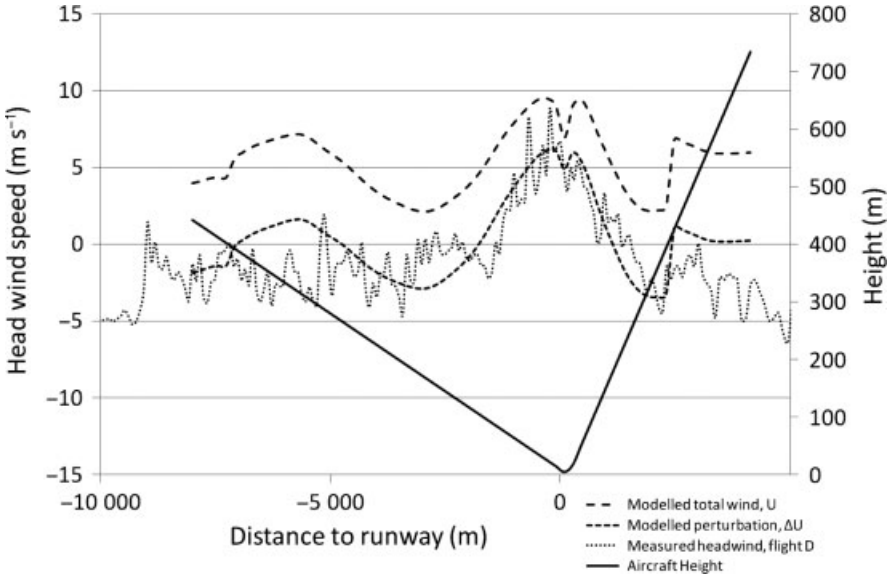

Figure 12. Results showing perturbation to the head wind, and the total head wind using an idealized upstream flow field for the case of $h_0 =$ 400 m, $\phi = 140^\circ$ and $\Delta T = 7.19\,^\circ$C. The dotted line is the measured head wind speed from the missed approach of flight D on 26 December 2009.

$h_0 = 700$ m. The figure shows that lower inversions give much higher wind speed perturbations with the range in speed being over 8 m s^{-1} for a 400 m inversion, but less than 4 m s^{-1} for an inversion height of 865 m. The height of the inversion has little impact on the location of the positive and negative perturbations.

For the purposes of comparing the model predictions with measured wind speeds, Figure 12 shows the calculated perturbation in the headwind for $h_0 = 400$ m, $\phi = 140^\circ$ and $\Delta T = 7.19\,^\circ$C and also this perturbation added to the idealized upstream profile used as input to the model. This provides an estimate of the total wind. The figure also shows the measured headwind provided for the missed approach of flight D on 26 December 2009. The model replicates the main features of the observed data with a peak in the headwind just upwind of the runway and a smaller peak some 6000 m upstream

7. Discussion

Figures 6 and 7 show that the observed structures of the flow in the aircraft approach are consistent with those observed by Shun and Lam (2002), in particular there are large changes in the speed of the flow parallel to the runways. Figures 9–12 show that the FLOWSTAR model, which represents the features of flow described in Section 2.1.4, also broadly predicts changes in the structure of the airflow parallel to the runway and that these changes are sensitive both to the upstream wind direction and the boundary layer height, and also (not presented) to the intensity of the inversion. It is important that the values of these parameters are optimized for the model to be used operationally as a predictive tool for wind shear. The reliability of the tool and confidence in its use will also be aided by further modelling studies and model enhancements to improve the understanding of the flow and the model performance. These could include the following.

1. Development of the model to account for the non-linear aspects of the flow of the inversion layer over the mountains of Lantau Island for example by using an iterative technique (CC). This approach will result in stronger downslope flows and hence larger wind shears, and may allow for hydraulic jumps downwind of the highest terrain and shear across the inversion layer as necessary.
2. The complex terrain on land to the north and east of Lantau may impact on the flow over Lantau for instance by channelling flow to the north of the island. This effect could be assessed by increasing the size of the FLOWSTAR domain. The model could also be used to estimate the extent to which topography in the vicinity of King's Park affects the wind speed and direction data from the radiosonde released at King's Park, especially in the lowest few hundred metres. This is important as these data are needed as input to the model.
3. Consideration of further physical processes including an assessment of the effects of upwind shear at inversion layers and hill wakes on the flow neighbouring HKIA, and determination of the extent to which unsteady wave/billows effect the flow (Tang *et al*., 2011). These processes could be parameterized within FLOWSTAR as necessary.
4. Verification of model improvements against the field data presented in the paper and other data as available.

Acknowledgements

Julian Hunt is grateful for support from Hong Kong University where he was a Distinguished Visiting Professor. A part of his research was conducted at the University of Notre Dame and was funded by Office of Naval Research Award # N00014-11-1-0709, Mountain Terrain Atmospheric Modeling and Observations (MATERHORN) Program.

References

Carruthers DJ, Choularton TW. 1982. Air-flow over hills of moderate slope. *Quarterly Journal of the Royal Meteorological Society* **108**(457): 603–624, DOI: 10.1002/qj.49710845708.

Carruthers DJ, Hunt JCR. 1990. Fluid mechanics of airflow over hills: turbulence, fluxes, and waves in the boundary layer. In *Atmospheric Processes in Complex Terrain*, Vol 23 Blumen W (ed.). American Meteorological Society: Boston, MA; 83–103.

Carruthers DJ, Hunt JCR, Weng W-S. 1988. A computational model of stratified turbulent airflow over hills – FLOWSTAR I. Proceedings of Envirosoft. In *Computer Techniques in Environmental Studies*, Zanetti P (ed.). Springer-Verlag: New York, NY; 481–492.

Chan PW. 2011. A significant wind shear event leading to aircraft diversion at the Hong Kong international airport. *Meteorological Applications* **19**: 10–16, DOI: 10.1002/met.242.

Cheung P, Lam CC, Chan PW. 2008. Numerical simulation of wind gusts in terrain-disrupted airflow at the Hong Kong international airport. *13th Conference on Mountain Meteorology*, 11–15 August 2008, Whistler, BC, Canada, http://www.hko.gov.hk/publica/reprint/r782.pdf (accessed 30 July 2012).

Coelho SLV, Hunt JCR. 1989. The dynamics of the near field of strong jets in crossflows. *Journal of Fluid Mechanics* **200**: 95–120.

Counihan J, Hunt JCR, Jackson PS. 1974. Wakes behind two-dimensional surface obstacles in turbulent boundary layers. *Journal of Fluid Mechanics* **64**: 529–564, DOI: 10.1017/S0022112074002539.

Hunt JCR, Delfos R, Eames I, Perkins RJ. 2007. Vortices, complex flows and inertial particles. *Journal of Flow, Turbulence and Combustion* **79**(3): 207–234. (volume in memory of Frans Nieuwstadt). DOI: 10.1007/s10494-007-9096-0.

Hunt JCR, Richards KJ, Brighton PWM. 1988. Stably stratified shear flow over low hills. *Quarterly Journal of the Royal Meteorological Society* **114**: 859–886, DOI: 10.1002/qj.49711448203.

Hunt JCR, Snyder WH. 1980. Experiments on stably and neutrally stratified flow over a model three-dimensional hill. *Journal of Fluid Mechanics* **96**: 671–704, DOI:10.1017/S0022112080002303.

Jackson PS, Hunt JCR. 1975. Turbulent wind flow over a low hill. *Quarterly Journal of the Royal Meteorological Society* **101**: 929–955, DOI: 10.1002/qj.49710143015.

Lapworth A. 2010. Jets on daytime boundary layer capping inversions. *Weather* **65**: 50–55, DOI: 10.1002/wea.424.

Lilly DK, Klemp JB. 1979. The effects of terrain shape on nonlinear hydrostatic mountain waves. *Journal of Fluid Mechanics* **95**: 241–261, DOI:10.1017/S0022112079001452.

Sheridan PF, Vosper SB, Mobbs SD. 2004. Rotors and downslope winds in the Falklands. *Bulletin of the American Meteorological Society* **85**: 1059–1060.

Shun CM, Lam HK. 2002. Remote sensing of wind shear under tropical cyclone conditions in Hong Kong. *The 35th Session of the Typhoon Committee*, 19–25 November 2002, Chiang Mai, Thailand, http://www.hko.gov.hk/publica/reprint/r485.pdf (accessed 30 July 2012).

Smith RB. 1979. The influence of mountains on the atmosphere. *Advances in Geophysics* **21**: 87–230, DOI: 10.1016/S0065-2687(08)60262-9.

Snyder WH. 1985. Fluid modeling of pollutant transport and diffusion in stably stratified flows over complex terrain. *Annual Review of Fluid Mechanics* **17**: 239–266, DOI: 10.1146/annurev.fl.17.010185.001323.

Tang W, Chan PW, Haller G. 2011. Lagrangian Coherent Structure Analysis of Terminal Winds Detected by Lidar. Part I: Turbulence Structures. *Journal of Applied Meteorological Climatology* **50**: 325–338, DOI: 10.1175/2010JAMC2508.1.

TOPFARM. 2011. Next generation design tool for optimization of wind farm topology and operation. Final activity report, EC contract no. TREN07/FP6EN/S07. 73680/03864, January 2011.

